# Splashing threshold of oblique droplet impacts on surfaces of various wettability

*Damon G. K. Aboud, Anne-Marie Kietzig**

Department of Chemical Engineering, McGill University, Montreal QC, H3A 0C5 Canada

KEYWORDS

Drop Impact, High-Speed, Tangential Velocities, Splashing Threshold, Drop Breakup, Wetting, Superhydrophobicity, Surface Roughness

Oblique drop impacts were performed at high speeds (up to 27 m/s, *We*>9000) with millimetric water droplets, and a linear model was applied to define the oblique splashing threshold. Six different sample surfaces were tested: two substrate materials of different inherent surface wettability (PTFE and aluminum), each prepared with three different surface finishes (smooth, rough, and textured to support superhydrophobicity). Our choice of surfaces has allowed us to make several novel comparisons. Considering the inherent surface wettability, we discovered that PTFE, as the more hydrophobic surface, exhibits lower splashing thresholds than the hydrophilic surface of aluminum of comparable roughness. Furthermore, comparing oblique impacts on smooth and textured surfaces, we found that asymmetrical spreading and splashing behaviours occurred under a wide range of experimental conditions on our smooth surfaces, however impacts

occurring on textured surfaces were much more symmetrical, and one-sided splashing occurred only under very specific conditions. We attribute this difference to the air-trapping nature of textured superhydrophobic surfaces, which lowers the drag between the spreading lamella and the surface. The reduced drag affects oblique drop impacts by diminishing the effect of the tangential component of the impact velocity, causing the impact behaviour to be governed almost exclusively by the normal velocity. Finally, by comparing oblique impacts on superhydrophobic surfaces at different impact angles, we discovered that although the pinning transition between rebounding and partial rebounding is governed primarily by the normal impact velocity, there is also a weak dependence on the tangential velocity. As a result, pinning is inhibited in oblique impacts. This led to the observation of a new behaviour in highly oblique impacts on our superhydrophobic surfaces which we named the stretched rebound, where the droplet is extended into an elongated pancake shape and rebounds while still outstretched, without exhibiting a recession phase.

## 1. INTRODUCTION

Droplet impacts on solid surfaces have been the subject of intensive study over the past few decades. A rich body of literature already exists considering perpendicular drop impacts, with a droplet falling from above onto a flat surface [1-8]. These studies have revealed the underlying mechanics and possible outcomes of droplet splashing and are industrially relevant to processes such as spray coating, spray cooling and inkjet printing. However, very few studies have been performed at oblique impact angles or at high impact velocities (over 10 m/s), relevant to engineering problems such as rain erosion on fast moving vehicles and turbine blades [9-11].

As a droplet impacts a solid surface, a thin lamella of water spreads around it, reaches a maximum extension, and then recedes back towards the center. It is the interaction of this lamella with the surface and the surrounding gas that ultimately defines the impact behaviour [1].

Impacting droplets may exhibit spreading behaviours such as deposition or receding breakup, or splashing behaviours such as prompt splashing, in which secondary droplets detach from the lamella during its spread across the surface, or corona splashing, in which the lamella first lifts off the surface onto a thin film of air, and then proceeds to destabilize into secondary droplets [2].

Droplet impacts on superhydrophobic (SHP) surfaces have gained recent attention because the non-wetting nature of such surfaces provokes entirely new impact behaviours such as rebounding, partial rebounding, and pancake bouncing [2, 3]. Superhydrophobicity is a surface's ability to easily repel water droplets and resist wetting. A SHP surface is defined by two caveats: an advancing contact angle ($\theta_A$) with water above 150°, and a contact angle hysteresis (CAH) below 10° [12]. This combination of properties is characterized by droplets sitting atop the peaks of rough features on the surface, leaving pockets of air below, which is known as the Cassie-Baxter wetting state.

For SHP surfaces, previous drop impact studies have focused primarily on the mechanics of the rebounding and partial rebounding impact behaviours [4, 13, 14]. At low impact speeds, droplets exhibit rebounding, in which the non-wetting properties of the SHP surface cause the lamella to recede back to its origin, recombine into a single droplet, and bounce off the surface. Although some partial penetration of the impacting liquid droplet into the textured surface occurs even at low impact velocities, higher speed impacts can cause a wetting transition at the impact center, from the Cassie to the Wenzel wetting state, in which the liquid is in complete contact with the solid. The threshold for this transition is governed by a competition between the anti-wetting Laplace pressure ($P_L$), which is a manifestation of the surface tension of the curved liquid interface as it penetrates into the pores of the textured surface, and the impalement pressure exerted by the droplet as it impacts the surface. The Laplace pressure is given by [15]:

$$P_L = \frac{2\sigma}{R_L} Cos(\theta_A) \quad (1)$$

where $R_L$ is the radius of curvature of the penetrating liquid, $\sigma$ is the surface tension and $\theta_A$ the advancing contact angle. By considering the air drainage mechanics below the impacting droplet, Maitra et al. (2013) found that the maximum impalement pressure exerted by the droplet onto the textured surface during impact, $P_{imp}$, is given by:

$$P_{imp} = 0.99 \frac{(D\mu_g^{-1} v_n{}^7 \rho^7 Ca)^{1/3}}{P_{atm} D^{1/2} St^{7/9}} \quad (2)$$

in which the Stokes and capillary numbers are defined as $St=2\mu_g/\rho v_n D$ (with $\mu_g$ the viscosity of air, $\rho$ the density of the liquid, $v_n$ the normal impact velocity, and $D$ the diameter of the drop), and $Ca=\mu_g v_n/\sigma$ [4]. Thus, for impacts occurring at a sufficiently high velocity, the impalement pressure exceeds the Laplace pressure, causing a Cassie-to-Wenzel wetting transition. However, as this transition is localized to only a small area at the impact center, the lamella spreads and recedes across the surface in the Cassie state [4]. This results in partial rebounding, such that when the lamella recombines and rebounds, the Wenzel-wet portion at the impact center is left behind, pinned to the surface.

All of the behaviours presented so far are well understood for droplets impacting normally on surfaces, but impact behaviours become much more complex in oblique impacts due to the asymmetry of the interaction. Thus, different splashing or spreading behaviours may occur at different locations around the radius of the impacting droplet, causing behaviours such as one-sided prompt splashing, one-sided corona splashing, or corona-prompt splashing, in which the two different types of splash are observed at opposite ends of the lamella [11]. In addition, drop impacts on moving surfaces may result in splashing behaviours unique to oblique impacts, such as the splashing rebound or aerodynamic breakup behaviours observed by Li (2013) [11].

Oblique droplet impacts are best described by considering the influence of the tangential velocity, $v_t$. **Figure 1** provides a 2D schematic illustrating the geometry of an oblique impact experiment, in which water droplets fall through the air at a velocity of $v_d$, and contact a surface travelling horizontally at $v_s$ and at a tilt angle of α. The frame of reference can be rotated so as to simplify the impact parameters to only the normal velocity of the droplet, $v_n = v_s Sin(\alpha) + v_d Cos(\alpha)$, and tangential velocity of the surface, $v_t = v_s Cos(\alpha) - v_d Sin(\alpha)$. In the following, we will refer to the edge of the lamella which spreads against the motion of the surface as the front of the lamella, and refer to the edge of the lamella which spreads with the motion of the surface as the tail.

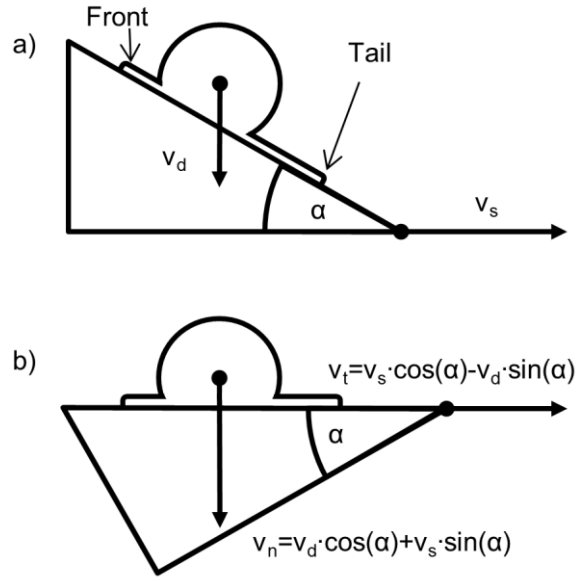


**Figure 1.** Schematic of oblique droplet impact.

For droplet impacts at a normal angle of incidence, the threshold of the onset of splashing ($K$) has traditionally been defined using the Weber number, $We = \rho {v_n}^2 D/\sigma$, and the Reynolds number, $Re = \rho v_n D/\sigma$, with $\mu$ the dynamic viscosity of the liquid. The splashing threshold ($K$) has been shown to follow the correlation [5, 16]:

$$We\sqrt{Re} = K \tag{3}$$

Thus, splashing occurs in droplet impacts where $We\sqrt{Re} > K$, and spreading occurs when $We\sqrt{Re} < K$. The splashing threshold must usually be found empirically for a given surface as it depends on several factors. The experiments of Stow and Hadfield (1981) as well as those of Range and Feuillebois (1998) have shown that rougher surfaces exhibit a lower value of *K*, and therefore more splashing [5, 6]. Xu (2005) found that decreasing the ambient gas pressure raises the splashing threshold, proving that the liquid's interaction with the ambient gas is essential for splashing to occur.

Bird et al. (2009) expanded on **Equation 3** in order to model the splashing threshold of oblique droplet impacts [17]:

$$We\sqrt{Re}(1 - \frac{v_t k}{v_n\sqrt{Re}})^2 = K \tag{4}$$

The parameter *k* is related to the lamella's spreading dynamics, such that $k=1/c$, where *c* is a constant relating the lamella's spread radius, $R_l$, to the normal impact velocity, in the relation [7, 17]:

$$R_l = 2c\sqrt{\frac{tv_n}{D}} \tag{5}$$

where *t* is the time elapsed since the moment of impact. For ethanol impacting obliquely on smooth glass, Bird et al. (2009) found that $K=5700$ and $k=2.5$ [17]. In **Equation 4**, the sign of the tangential velocity, $v_t$, is taken with respect to the spreading direction of the lamella. Therefore, $v_t$ is negative for the front of the lamella (as per **Figure 1**), which spreads against the direction of the oncoming surface, and positive for the tail end, which spreads in the same direction as the surface's motion. Thus, considering a frame of reference as shown in **Figure 1**, two splashing thresholds can be

differentiated, one for each extreme of the spreading lamella. In this way, two-sided splashing, one-sided splashing, and spreading on both sides can be distinguished.

Many oblique impact studies, such as those performed by Sikalo et al. (2005) and Liu et al. (2010), have been performed by dripping water onto a tilted substrate [18, 19]. In these experiments, both the normal and tangential impact velocities were limited to the terminal velocity of water droplets in air, around 4 m/s. In order to study the effects of higher tangential velocities, several studies have been conducted by dripping water onto rotating disks. This method has been employed by Povarov et al. (1976), Mundo et al. (1995), Chen and Wang (2005), Ghai et al. (2010), Fathi et al. (2010), Zen et al. (2010), and Bird et al. (2009) [16, 17, 20-24]. Although these experiments reached high tangential velocities, the normal velocity was still restricted to below 4 m/s. To exceed this limitation, Li (2013) accelerated an aluminum surface up to speeds as high as 63 m/s, and performed drop impacts at several tilt angles [11].

Each of the oblique impact studies listed above were performed using only one surface, which leaves the influence of the surface wettability on the oblique impact behaviour uninvestigated. Furthermore, although several studies, such as those by Young et al. (2014) and Ramachandran et al. (2015), have investigated impacts on angled, stationary SHP surfaces [13, 14], an investigation of the behaviour of droplets in high-speed, oblique impacts on SHP surfaces has not yet been reported. Thus, our experiments investigate the impact behaviour and splashing threshold of high-speed (up to 27 m/s), oblique impacts of millimetric droplets on six different surfaces: two substrate materials of different inherent surface wettability (PTFE and Al), each prepared with three different surface finishes (smooth, rough, and textured), allowing us to compare the behaviour on surfaces with wetting behaviours ranging from hydrophilic to superhydrophobic. The goals of this report are to investigate the role of the surface wettability and roughness on splashing,

to comprehensively determine the possible splashing behaviours in oblique impacts, and to define the thresholds between those behaviours.

## 2. EXPERIMENTAL

Smooth aluminum and PTFE sample surfaces were prepared by polishing with 600 and then 1200 grit SiC polishing disks. The rough surfaces were prepared by sanding using 40 grit sandpaper. The SHP PTFE surface was fabricated using femtosecond laser micromachining, replicating the process used by Liang et al. (2014) [25]. A Coherent Libra amplified Ti:Sapphire laser with a wavelength of 800 nm, pulse duration shorter than 100 fs, and repetition rate of 10 kHz was used to irradiate polished PTFE samples. Using a focal spot size of 36.9 μm (with an effective line width of 24.1 μm), textured PTFE surfaces were synthesized by raster scanning with a peak fluence of 2.06 J/cm$^2$ and a 78% line overlap. The irradiation process induced complex nanoscopic surface textures, which, when combined with the low surface energy of the PTFE, result in a SHP surface, as reported by Liang et al. (2014) [25]. The SHP aluminum surface was prepared by sputtering a 50 nm thin film of aluminum onto a SHP PTFE surface. The textured surfaces were attached onto aluminum sample holders using epoxy. **Figure 2** provides scanning electron microscope images (Hitachi S-3700) of all six surfaces tested.

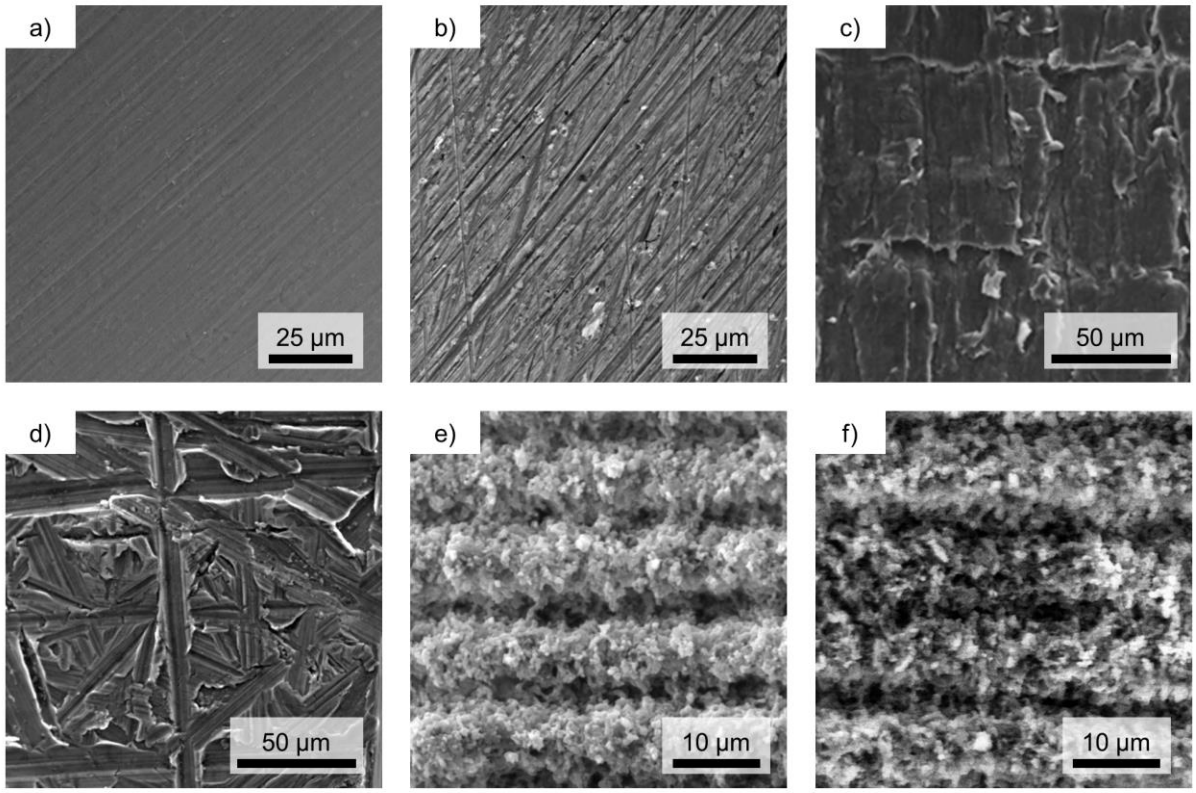


**Figure 2.** SEM micrographs of each surface. (a) smooth PTFE, (b) smooth aluminum, (c) rough PTFE, (d) rough aluminum, (e) textured PTFE, (f) textured aluminum.

Droplets were produced using a drop-on-demand (DOD) generator based on the design published by Cheng and Chandra (2003) [26]. We used a 55 mL polypropylene syringe with a dispense tip as the water reservoir. A solenoid valve introduced pulses of nitrogen gas into the reservoir, producing a single droplet at the dispense tip. A vent at the top of the reservoir allowed the excess pressure to escape. Generated droplets were formed with negligible downwards velocity, and fell approximately 4 cm before impact. During their fall, any oscillations imparted on the droplets through their formation process by the DOD ceased due to viscous dissipation, resulting in spherical droplets. This process is shown in Supporting Figure S1. Using a 150 µm inner diameter stainless steel dispense tip and a 16 µs gas pulse at 180 psi, the DOD produced 0.95

mm diameter droplets. Using a 330 μm inner diameter PTFE-lined dispense tip and 10 μs gas pulses at 37 psi, the DOD produced 1.3 mm diameter droplets. Although some images are provided for larger droplets in order to provide better resolution, our main analysis is performed using water droplets of a uniform diameter of $D$=0.95 mm.

A 3D illustration of the experimental setup is shown in **Figure 3**. A pneumatic accelerator controlled the sample speed. This setup consists of a piston and chamber assembly, with the sample attached to a sample holder mounted at the end of the piston, which was driven using pneumatic pressure in the range of 100-1000 psi. To achieve sample speeds greater than 16 m/s, the double diaphragm ballistics method was employed. Using this method, 2.54 cm Mylar polymer diaphragms of 25 or 50 μm thickness allowed a sudden rush of gas pressure to enter the piston chamber upon rupture resulting in sample velocities up to 27 m/s. A Photron SA5 high speed camera captured the videos using an 18-108 mm Navitar Macro Zoom 7000 lens. Backlighting was provided by a AI SL185-WHI-IC Ultra Bright Spot Light (Optikon Corp.). LabView was used to trigger the camera and the pneumatic valves controlling the accelerator and DOD device. Between each experimental run, samples were rinsed with acetone and allowed to dry.

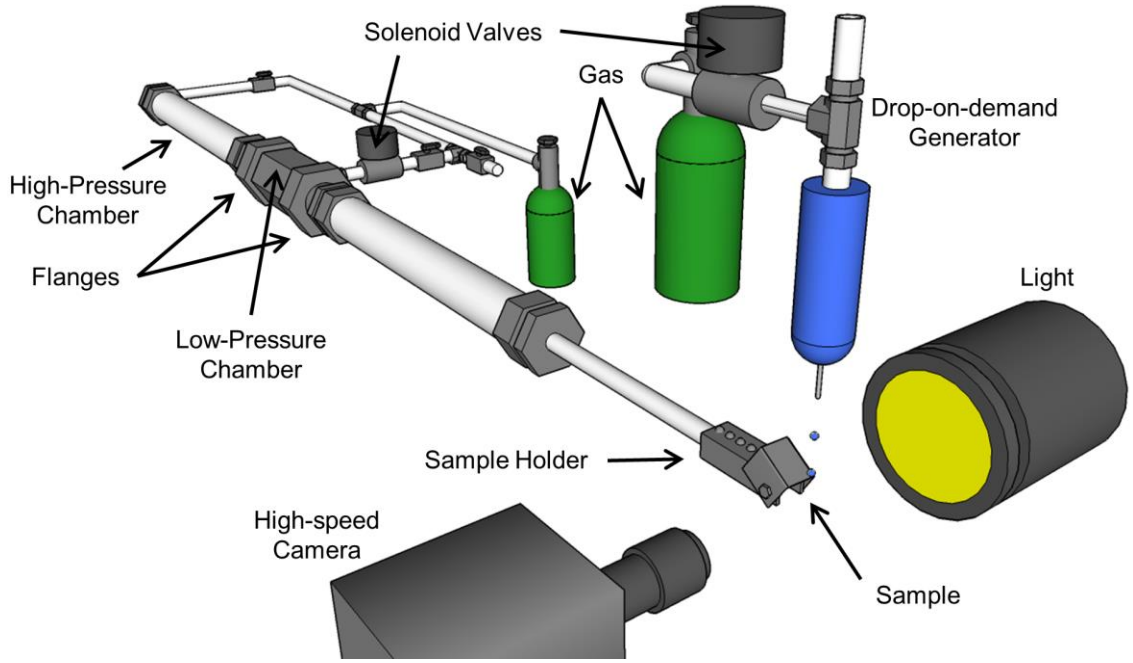


**Figure 3.** 3D illustration of the experimental setup.

The average roughness ($R_a$) of the sample surfaces was characterized using a Dektak 3ST surface profilometer, manufactured by Veeco. Mean values were determined by profiling seven 5 mm sections on the samples at a stylus force of 10 mN, at a spatial sampling frequency of 0.5 μm. Each sample was cleaned ultrasonically in acetone and dried under a heat lamp before their advancing and receding contact angles were measured using a Data Physics OCA 15E goniometer. For dynamic contact angle measurements, the volume of the droplet was increased at a rate of 0.2 μL/s from 2 μL to 7 μL, and then after a 5 second pause the volume was reduced back to 2 μL at the same rate. The reported values are averaged from 5 measurements from different locations on the sample surfaces.

Model fitting and determination of the associated 95% confidence intervals (CIs) was performed using logistic regression. In the following, confidence intervals are presented as "mean [lower confidence limit; upper confidence limit]".

## 3. RESULTS & DISCUSSION

Droplet impacts were tested on six surfaces: smooth, rough, and textured PTFE, as well as smooth, rough, and textured aluminum. Throughout this report, we will refer to these surfaces as s-PTFE, r-PTFE, t-PTFE, s-Al, r-Al, and t-Al for brevity. **Table 1** provides the roughness ($R_a$) and wetting properties of each of the six surfaces tested. In the discussion below, we will refer to the smooth and rough surfaces as regular surfaces, and to the textured surfaces as SHP surfaces. Also, note that although the conditions of drop impacts are typically presented in terms of the Weber number, we chose not to adimensionalize our results. This is because we observed that the effect of the tangential velocity on the impact behaviour does not change predictably with changes in drop diameter, and also the effect of the viscosity and surface tension are still unclear. Thus, using the Weber or Reynolds numbers to represent the tangential velocity would be misleading. Time, however, will be presented dimensionless as $t^*=t \cdot v_n/D$ for temporal comparison among behaviours.

**Table 1.** Surface characteristics.

| | Smooth PTFE | Rough PTFE | Textured PTFE | Smooth aluminum | Rough aluminum | Textured aluminum |
|---|---|---|---|---|---|---|
| Abbreviation | s-PTFE | r-PTFE | t-PTFE | s-Al | r-Al | t-Al |
| $R_a$ (nm) ± 2 st. dev. | 16 ± 6 | 1070 ± 250 | N/A* | 62 ± 23 | 1140 ± 240 | N/A* |
| $\theta_A$ ± 2 st. dev. | 107 ± 3° | 124 ± 3° | 157 ± 3° | 71 ± 6° | 82 ± 6° | 157 ± 2° |
| $\theta_R$ ± 2 st. dev. | 80 ± 4° | 80 ± 5° | 156 ± 3° | 16 ± 6° | 8 ± 3° | 154 ± 2° |

### 3.1. DESCRIPTIONS OF OBLIQUE IMPACT BEHAVIOURS

A total of twelve distinct behaviours were observed for droplet impacts on regular and SHP surfaces. For each of the six different surfaces tested, **Figure 4** plots the experimental conditions

under which each behaviour was observed, with respect to the velocity ($v_s$) and tilt angle (α) of the surface (as illustrated in **Figure 1(a)**). All of the data in this figure is for droplets of an average diameter of 0.95 ± 0.4 mm (avg. ± 2 st. dev.).

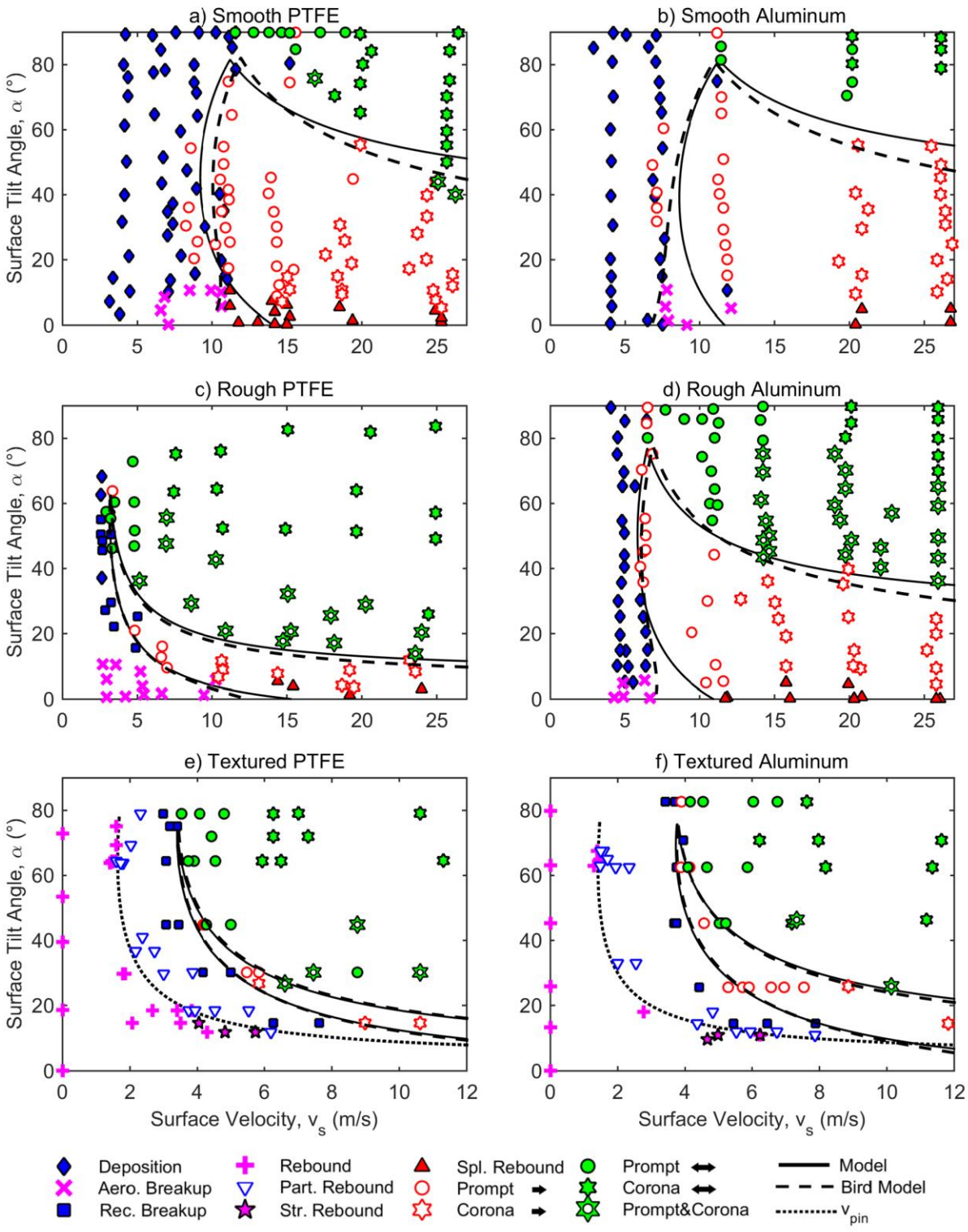
a) Smooth PTFE
b) Smooth Aluminum
c) Rough PTFE
d) Rough Aluminum
e) Textured PTFE
f) Textured Aluminum
Surface Tilt Angle, α (°)
Surface Velocity, v_s (m/s)
Deposition
Aero. Breakup
Rec. Breakup
Rebound
Part. Rebound
Str. Rebound
Spl. Rebound
Prompt
Corona
Prompt
Corona
Prompt&Corona
Model
Bird Model
v_pin

**Figure 4**. Observed impact behaviours and applied models** for 0.95 mm diameter water droplets. For prompt and corona splashing, the arrows in the legend designate whether the marker indicates one- or two-sided splashing.

**Figure 5** provides snapshots of nine unique drop impact behaviours on regular surfaces (the original high-speed videos of each behaviour on regular and SHP surfaces are available in the supporting information for the interest of the reader). The deposition, receding breakup, two-sided prompt splash, and two-sided corona splash behaviours are shown in **Figure 5(a-d)**. Since these behaviours are well documented, we will not describe them here. Instead, we refer the reader to the review of Yarin (2006) for a comprehensive explanation of each behaviour [27]. In contrast to these symmetrical behaviours, impacts occurring with a significant tangential velocity are oblique, and result in asymmetrical behaviours. Aerodynamic breakup is shown in **Figure 5(e)** ($v_n$=1.66, $v_t$=9.44 m/s, $D$=1.36 mm), and occurred in drop impacts with low $v_n$ and moderate $v_t$. The droplet initially deposits on the surface and spreads into an elongated pancake shape due to the tangential motion of the surface (as seen at $t^*$=1.80). The front end then destabilizes due to a similar process as that described by Rayleigh-Plateau instability [11] and forms a bulge ($t^*$=3.31), eventually pinching off one large secondary droplet, which detaches from the lamella and surface ($t^*$=4.15). In impacts occurring at similarly low $v_n$, but at very high $v_t$, we observed splashing rebound, as shown in **Figure 5(f)** ($v_n$=1.85, $v_t$=20.42 m/s, $D$=0.96 mm) on smooth aluminum. By $t^*$=0.73, the front end of the lamella begins to lift off the surface into a splashing wave front, initially behaving much like a corona splash. However, there is a crucial difference between these two behaviours. In corona splashing, the furthest extent of the lamella front destabilizes into secondary droplets, whereas in the case of splashing rebound, the lamella detaches entirely from the surface ($t^*$=1.95),

and proceeds to recombine upon itself driven by surface tension, eventually forming a large secondary droplet ($t^*$=2.92). In oblique impacts at higher $v_n$, we observed one-sided prompt splashing, as shown in **Figure 5(g)** ($v_n$=7.40, $v_t$=11.48, $D$=1.38 mm). Impacts occurring at even higher $v_t$ exhibited one-sided corona splashing, as seen in **Figure 5(h)** ($v_n$=7.40, $v_t$=26.2, $D$=0.96 mm). At very specific settings, it is possible for an impacting droplet to exhibit both prompt and corona splashing at different locations. **Figure 5(i)** ($v_n$=5.54, $v_t$=6.73, $D$=0.96 mm on r-PTFE) depicts the corona-prompt splash, in which a corona splashing occurs at the front end of the lamella, and prompt splashing at the tail end.

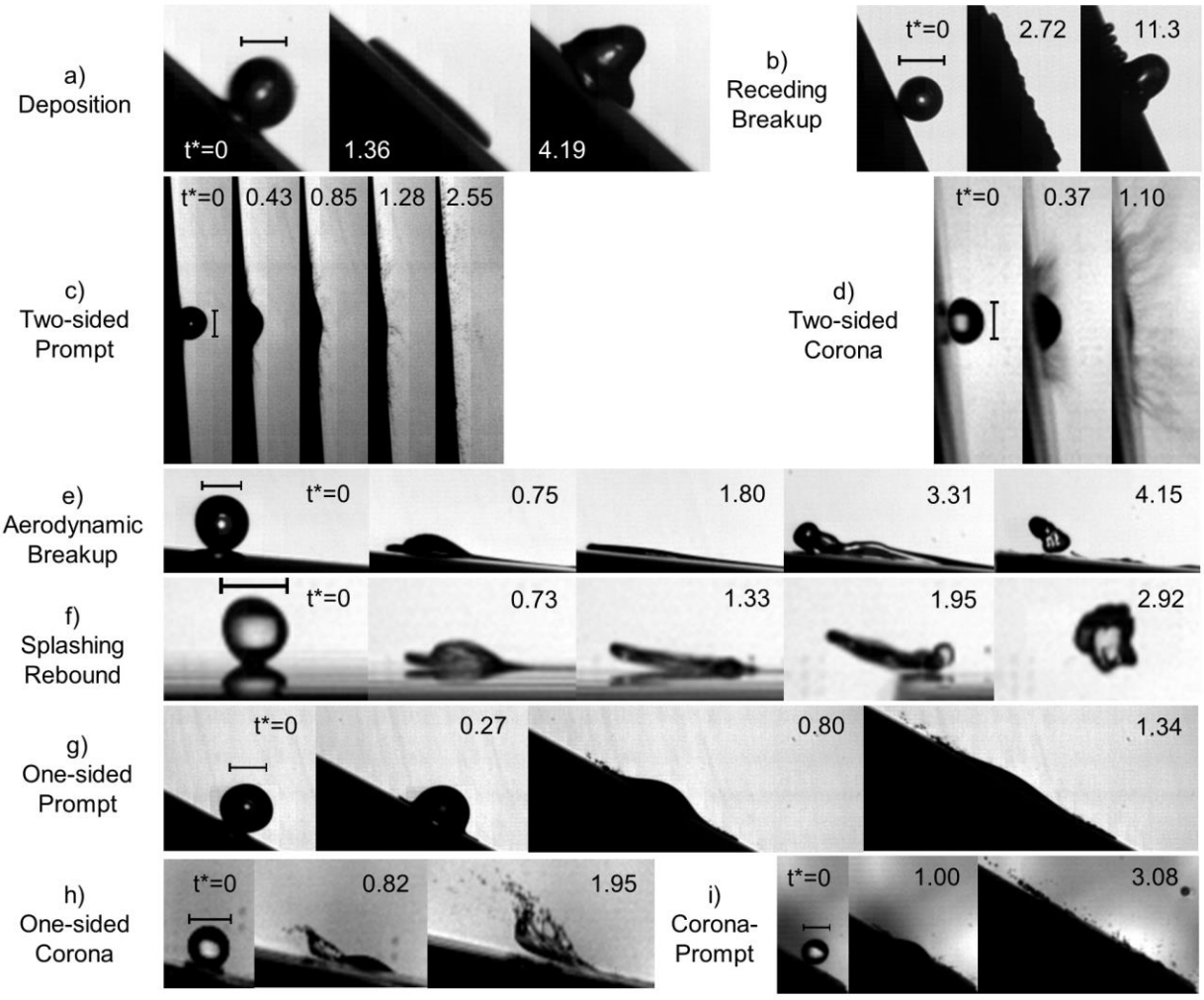

**Figure 5.** Observed impact behaviours on regular surfaces. All images are for the s-PTFE surface except (b) on r-PTFE and (f) on s-Al. Each scale bar is 1 mm in length. The velocities (m/s) and drop diameters (mm) are: a) $v_n$=1.42, $v_t$=0.42, $D$=1.36. b) $v_n$=2.97, $v_t$=2.04, $D$=0.97. c) $v_n$=16.26, $v_t$=0.44, $D$=1.27. d) $v_n$=25.89, $v_t$=1.07, $D$=0.94. e) $v_n$=1.66, $v_t$=9.44, $D$=1.36. f) $v_n$=1.85, $v_t$=20.42, $D$=0.95. g) $v_n$=7.40, $v_t$=11.48, $D$=1.38. h) $v_n$=7.40, $v_t$=26.20, $D$=0.96. i) $v_n$=5.54, $v_t$=6.73, $D$=0.96.

Neither deposition nor aerodynamic breakup were observed on our textured surfaces, due to their non-wetting nature. However, many of the same impact behaviours were seen, including: receding breakup, prompt splashing, corona splashing, corona-prompt splashing, and splashing rebound, as shown in **Figure 6(d-j)**. In addition, drop impacts on our SHP surfaces resulted in three behaviours that were not observed on our regular surfaces. **Figure 6(a)** depicts rebounding ($v_n$=1.64, $v_t$=2.36 m/s, $D$=1.29 mm). After the lamella reaches maximum extension ($t^*$=2.48), it retracts back towards its center and recombines, bouncing off the surface entirely ($t^*$=4.95). At higher normal velocities, a Cassie-to-Wenzel wetting shift occurred at the impact center due to the high impalement pressure, resulting in partial rebounding, as seen in **Figure 6(b)** ($v_n$=1.71, $v_t$=0.04 m/s, $D$=1.34 mm). The lamella retracts and the droplet rebounds from the surface ($t^*$=5.89), but a small secondary droplet remains behind, pinned to the surface ($t^*$=8.01).

In impacts occurring at a low enough normal velocity to prevent pinning but with high tangential velocity, we observed a new behaviour, which we call the stretched rebound, as shown in **Figure 6(c)** ($v_n$=1.66, $v_t$=4.44, $D$=1.36 mm). In this scenario, the motion of the surface stretches the impacting droplet into an elongated pancake shape. The entire droplet then detaches from the surface while still outstretched ($t^*$=2.86 to 3.95). After its release from the surface, we observed destabilization of the deformed, rebounded droplet, forming a chain of secondary droplets ($t^*$=4.99). The stretched rebound behaviour is very similar to the pancake bouncing behaviour

observed by Liu et al. (2014) [3]. In the case of pancake bouncing, when the liquid that partially penetrates into the pores of the surface at the impact center is ejected by capillary forces, its momentum forces the impacting droplet back upwards, lifting the entire droplet off the surface while still outstretched in a pancake shape. In contrast, since we observed stretched rebound occurring at high tangential velocity, the rebounding droplet translated laterally across the surface during its spread, and detached from the surface at a location well away from its impact center. In the case of the stretched rebound shown in **Figure 6(c)**, the droplet translated 11 mm across the surface before detaching, such that the tail of the lamella was over 8 mm away from the impact center. Therefore, since the droplet's detachment was independent of the capillary ejection at the impact center, it is clear that the stretched rebound is a unique impact behaviour.

This assertion is confirmed by an analysis of the rebounding timescale of the two behaviours.The total contact time with the surface for rebounding droplets, $\tau_{reb}$, has been shown to follow the relation:

$$\tau_{reb} = \beta \sqrt{\frac{\rho R^3}{\sigma}} \tag{6}$$

with $R$ the droplet radius, and $\beta$ a scaling factor [28]. Apart from some exceptional cases [3, 29], most SHP surfaces exhibit contact times comparable to that found by Biance et al. (2006), who reported that $\beta$=2.65 [3, 28, 30]. Liu et al. (2014) found an exceptionally low timescale of $\beta$=0.53 for pancake bouncing [3], whereas we observed a significantly longer timescale for stretched rebound, with $\beta$=1.32. This dramatic difference in timescale indicates that the underlying mechanism is quite different. Still, since the stretched rebound behaviour did not involve a retraction phase, we found that it did occur significantly faster than rebounding, for which we found $\beta$=1.81.

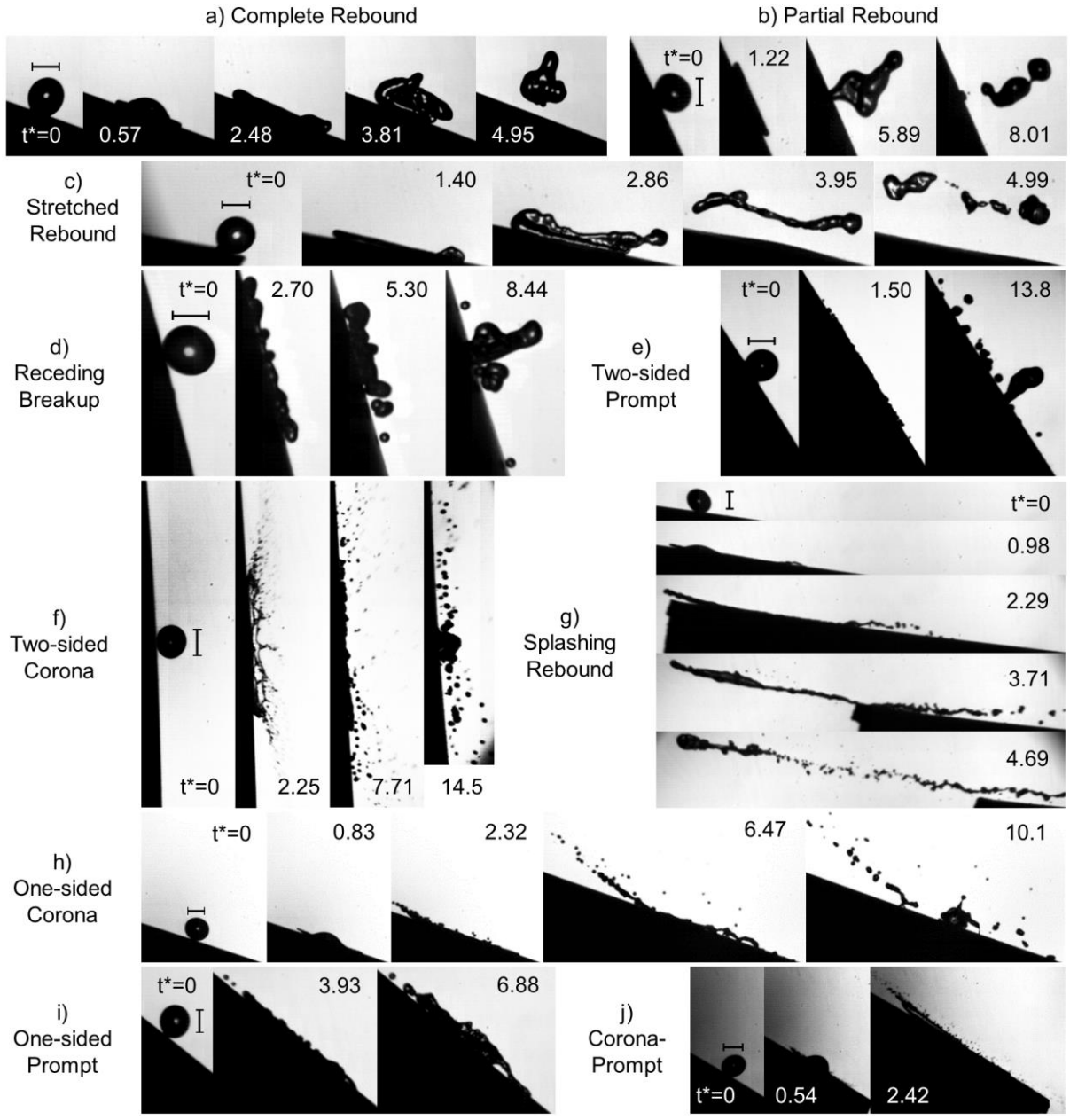


**Figure 6.** Observed impact behaviours on SHP surfaces. All images are taken from the t-PTFE surface except (c) and (d) on t-Al. Each scale bar is 1 mm in length. The velocities (m/s) and drop diameters (mm) are: a) $v_n$=1.64, $v_t$=2.36, $D$=1.29. b) $v_n$=1.71, $v_t$=0.04, $D$=1.34. c) $v_n$=1.66, $v_t$=4.44, $D$=1.36. d) $v_n$=2.91, $v_t$=0.03, $D$=1.34. e) $v_n$=4.20, $v_t$=1.73, $D$=1.26. f) $v_n$=8.70, $v_t$=0.32, $D$=1.35. g)

$v_n$=2.95, $v_t$=16.03, $D$=1.35. h) $v_n$=4.50, $v_t$=10.63, $D$=1.35. i) $v_n$=3.64, $v_t$=2.26, $D$=1.30. j) $v_n$=7.39, $v_t$=10.47, $D$=1.37.

## 3.2. MODELLING THE SPLASHING THRESHOLD

In order to model the splashing threshold, we first define which behaviours are indeed splashing behaviours, and which are non-splashing. In previous reports, **Equations 3** and **4** were used to define the onset of prompt or corona splashing for impacting droplets [5, 16, 17]. Following this logic, we consider only prompt- and corona-type splashing (including splashing rebound) as splashing behaviours, and all of the other behaviours as non-splashing. Therefore, splashing is understood as the formation of a splashing wave front or of secondary droplets during the lamella's spreading phase over the surface. This definition is not met by receding breakup, in which secondary droplets are produced during the lamella's recession, as opposed to its spreading phase. Similarly, both stretched rebound and aerodynamic breakup result in the disintegration of the bulk liquid, but by mechanisms very different than prompt or corona splashing. Thus, the latter three behaviours fall under the non-splashing category.

Given this definition of splashing, we found that the splashing threshold (*ST*) could be accurately modelled using the equation:

$$ST = v_{n0} + mv_t \tag{7}$$

where $v_{n0}$ is the critical velocity for splashing at a normal angle of incidence, $m$ defines a slope with respect to $v_t$, and splashing occurs for cases in which $v_n > ST$. **Figure 7(a)** provides an illustration of how **Equation 7** can be interpreted graphically. Following the logic of Bird's oblique splashing model (**Equation 4)**, $v_t$ is defined as the surface's velocity with respect to the lamella's spreading direction. Therefore, a single droplet impact will be represented by two points on the plot at mirrored positions across the $v_t$=0 line: one on the left representing the behaviour at the lamella's front, and one on the right representing the tail. For example, a droplet impact exhibiting one-sided corona splashing should be represented by one point above the model line on

the left, and one point below the model line on the right, as indicated by the dashed circles in the figure. For two-sided splashing, both points should be located above the model line, and non-splashing impacts should be given by two mirrored points below the line.

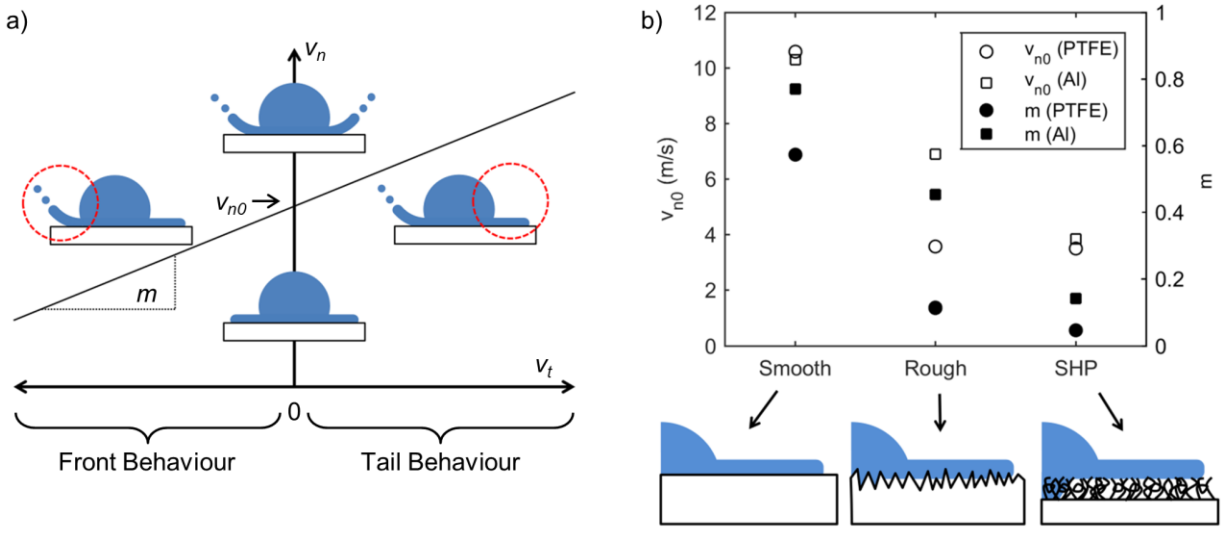


**Figure 7.** a) Illustration of the types of splashing behaviours separated by our model. b) Dependence of modelling parameters from **Equation 7** (normal splashing threshold, $v_{n0,}$ and the slope, $m$) on surface finish. The diagrams below qualitatively illustrate the solid fraction of the spreading lamella for each surface structure.

**Figure 8** displays the fit for **Equation 7** for each of the six surfaces tested, and **Table 2** provides the associated modelling parameters. Overall, **Equation 7** provided a good fit in each case. The only surfaces which show major deviation from the model are the s-PTFE and s-Al surfaces. Notably, for s-PTFE, several of the splashing rebound points are located below the model line, in the non-splashing region. Many of the inconsistencies seen in the model fit for the smooth surfaces are likely due to lodged dust particles on the surfaces. Our polished PTFE and aluminum surfaces were polished to $R_a$ of 16 nm and 62 nm, respectively (as per **Table 1**). Stow and Hadfield (1981)

showed that the splashing threshold is extremely sensitive to slight changes in roughness for well-polished surfaces [5]. Although the surfaces were cleaned between each experiment, dust particles may have become lodged on the surface during its motion towards the droplet. Such particles on the surface would provoke splashing in impacts occurring very near them, and therefore create error in the splashing threshold. This factor would have a lessened effect on the rough and lased surfaces, since small particles would not significantly affect the overall roughness, and therefore the results were more consistent.

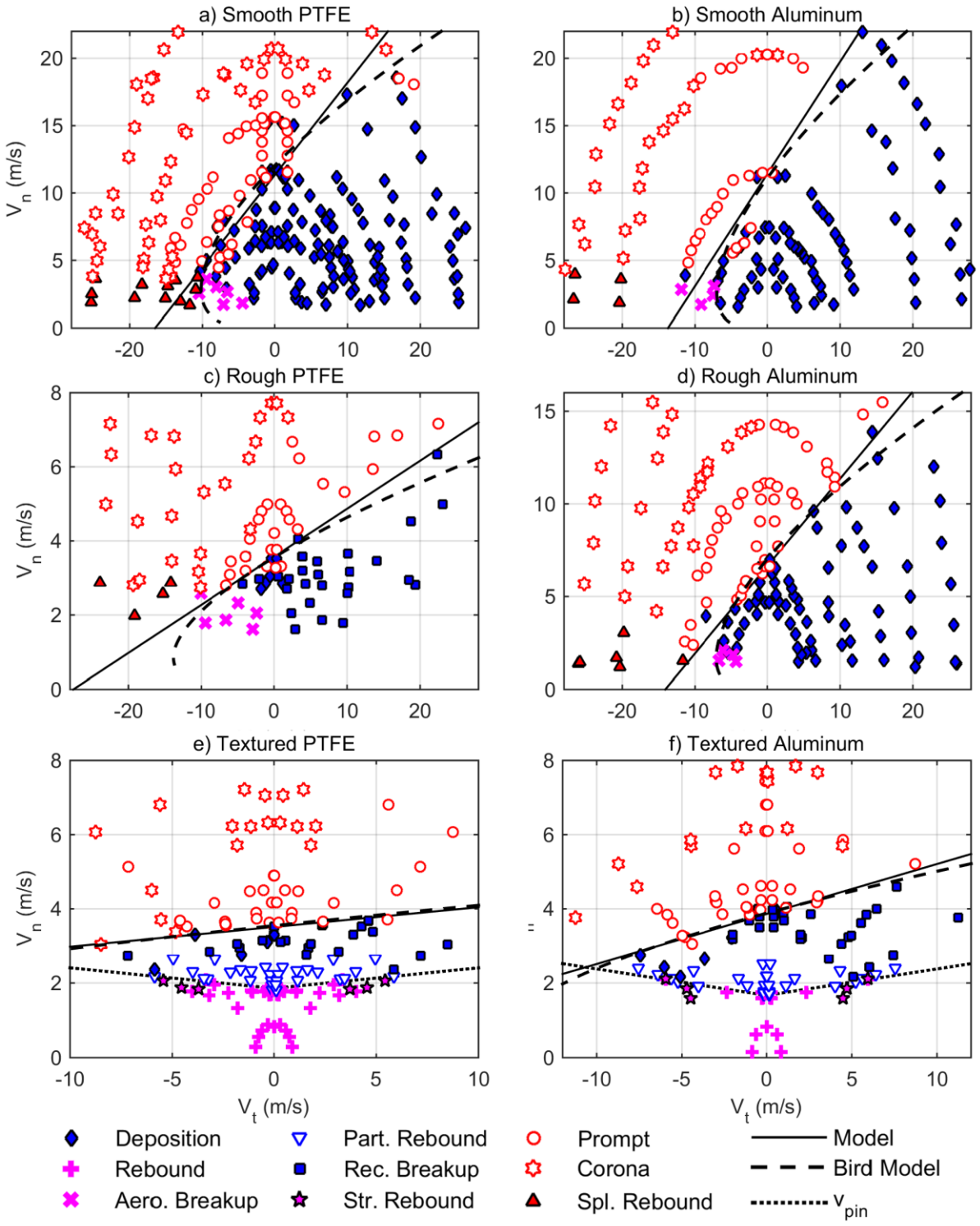


**Figure 8**. Observed behaviours*** and application of models for the splashing threshold of oblique impacts of 0.95 mm diameter droplets.

**Table 2.** Modeling Parameters.

| Surface | D (mm) ± 2 st. dev. | Model [95% CI] $v_{n0}$ | m | Bird's Model K | k |
|---|---|---|---|---|---|
| s-PTFE | 0.93 ± 0.04 | 11.33 [10.23; 12.43] | 0.69 [0.54; 0.84] | 197,000 | 72.8 |
| r-PTFE | 0.97 ± 0.02 | 3.57 [3.35; 3.79] | 0.13 [0.10; 0.16] | 9,930 | 8.77 |
| t-PTFE | 0.97 ± 0.09 | 3.51 [3.43; 3.59] | 0.053 [0.019; 0.087] | 9,420 | 4.18 |
| s-Al | 0.94 ± 0.02 | 11.42 [10.32; 12.52] | 0.83 [0.64; 1.02] | 163,000 | 94.9 |
| r-Al | 0.94 ± 0.02 | 6.64 [6.35; 6.93] | 0.47 [0.41; 0.53] | 51,900 | 47.2 |
| t-Al | 0.97 ± 0.06 | 3.86 [3.74; 3.98] | 0.13 [0.10; 0.16] | 11,810 | 9.40 |

**Figure 7(b)** illustrates the observed changes in the modelling parameters among the surfaces tested. We will begin by discussing the normal splashing threshold, and then consider the slope of our model. A high value of the normal splashing threshold, $v_{n0}$, indicates a surface which inhibits splashing. Comparing the smooth and rough surfaces, we see that the normal splashing thresholds of $v_{n0}$=11.3 and 11.4 m/s on the smooth surfaces are much greater than those of 3.57 and 6.64 m/s for the rough PTFE and aluminum surfaces, respectively. These values indicate that splashing is encouraged on rough surfaces, which is consistent with the observations of Stow and Hadfield (1981) and Range and Feuillebois (1998) [5, 6].

Considering the differences between the two materials in the normal splashing thresholds for each surface topology, we observe a significant difference for the rough surfaces, while the smooth and patterned surfaces show very similar thresholds. In the following, we will first compare the rough and textured surfaces and close with the smooth surfaces. For the rough aluminum and PTFE surfaces, which had comparable $R_a$ values of 1140 and 1070 nm respectively, we found a splashing

threshold of $v_{n0}$=6.64 m/s on r-Al, exceeding the value of $v_{n0}$=3.57 m/s on r-PTFE by a factor of around two. This effect likely stems from the difference in wetting properties between the two materials. Since PTFE is inherently hydrophobic, the r-PTFE surface had an advancing contact angle of $\theta_A$=124°, much greater than the advancing contact angle of 82° for the r-Al surface (as per **Table 1**). Given the comparable roughness values, these results indicate that splashing is encouraged on more hydrophobic surfaces. This is a crucial discovery since in most splash threshold reports to date [16, 31-33], the effect of the inherent surface chemistry has not been considered when comparing the splashing threshold on different surfaces.

Where the normal splashing thresholds diverge by a factor of two between the rough aluminum and PTFE surfaces, the thresholds of $v_{n0}$=3.51 and 3.86 m/s for the textured PTFE and aluminum surfaces (respectively) differ by only 10%, indicating that surface chemistry has a lesser influence on the result on the splashing threshold on SHP surfaces. We attribute this to the low solid-liquid surface fraction ($f$) in the Cassie wetting state of the lamella. The value of $f$ denotes the fraction of the lamella's contact area with the solid surface, and can be calculated using the Cassie-Baxter equation [34]:

$$cos\theta_C = f(cos\theta_Y + 1) - 1 \tag{8}$$

where $\theta_C$ is the contact angle of the liquid on the textured surface, and $\theta_Y$ is the Young's contact angle of the surface material. Use of this equation requires caution, since the assumptions behind the Young's contact angle entail a surface which is atomically flat, chemically inert, chemically homogeneous, and perfectly rigid, which is impossible for any real surface. For the ease of comparison [35], we approximate $\theta_Y$ using the advancing contact angle ($\theta_A$) on our smooth surfaces, and thus roughly estimate the solid-liquid surface fraction from **Equation 8**. We measured values of $\theta_A$=157° on both t-Al and t-PTFE, leading to estimated surface fractions of

$f$=0.06 and 0.11, respectively. Therefore, on these surfaces, only a small fraction of the lamella actually interacted with the solid surface, whereas the majority of the lamella spread over trapped air pockets, which explains the small difference in the normal splashing threshold of our textured surfaces.

Next, we consider the change in the model's slope, $m$, among the surfaces tested. This parameter quantifies the prominence of the tangential velocity in affecting the oblique drop impact behaviour. Thus, on surfaces with relatively high values of $m$, such as s-PTFE (m=0.69), the tangential velocity greatly affects the impact behaviour, and one-sided splashing occurs under a wide range of conditions (see **Figure 8(a)**). In contrast, we found an exceptionally low value of $m$=0.053 for the t-PTFE surface. As a result, the impact behaviour on this surface was governed almost exclusively by the normal velocity, and the magnitude of $v_t$ had barely any effect on the behaviour at all. It is for this reason that very few cases of one-sided splashing were observed on this surface (see **Figure 8(e)**).

The fact that $m$ dropped by over an order of magnitude among the smooth, rough, and textured PTFE surfaces respectively begs the question: why does surface topology change its prominence in affecting the oblique behaviour? We suggest that this difference reflects the solid fraction of the spreading lamella. **Figure 7(b)** provides an illustration of the solid fraction for each surface structure. For drop impacts on the smooth PTFE surface, the lamella spread in full contact with the solid ($f \approx 1$), whereas for our t-PTFE surface, we estimated a solid-liquid surface fraction of only $f \approx 0.11$. In fact, recent work by Kim et al. (2014) suggests that even on our r-PTFE surface, the lamella spreads primarily atop the rough peaks in a temporary Cassie-like state, leaving channels of air beneath [8]. It is safe to assume that in the case of this rough surface, the solid fraction of the spreading lamella was at an intermediate value between that of its smooth and

textured counterparts and, therefore, that the value of $m$ decreased monotonically for surfaces exhibiting lower solid fractions in our experiments. A low solid fraction reduces the magnitude of $m$ because the conventional no-slip boundary condition for fluid flow over a solid is no longer valid on an air-trapping surface [36]. On such surfaces, only the solid fraction of the lamella is subject to the no-slip condition (and is hence dragged by the tangential motion of the surface), while the remaining fraction flows over trapped air, experiencing minimal drag, which explains why the tangential velocity of the surface had a diminished effect on the impact behaviour for the rough and textured surfaces tested.

The value of $m$ was also affected by the inherent surface chemistry. For the r-Al surface, we found that $m$=0.47, exceeding the slope of $m$=0.13 for the more hydrophobic r-PTFE surface by a factor of about four. The same trend is observed when comparing the textured surfaces, where the slope of 0.13 observed on the t-Al surface is much higher than the slope of 0.053 observed on the t-PTFE surface. These results indicate that the surface chemistry drastically affects the oblique impact behaviour, such that more hydrophilic surfaces are more affected by the tangential velocity.

As a point of interest, note that the smooth PTFE and aluminum surfaces have very similar modelling parameters ($v_{n0}$ and $m$), which is odd considering that they have different wetting properties and roughnesses. Where the smooth PTFE surface was more hydrophobic, the smooth aluminum surface was slightly rougher. Our discussion has shown that both roughness and increased hydrophobicity promote lower values of $v_{n0}$ and $m$. It appears that in this case, these two competing factors nearly negated each other, resulting in very similar oblique splashing thresholds on both surfaces.

Bird's model (**Equation 4**) was also included in **Figure 8** for comparison. However, it is important to note that, in order to apply Bird's model to our experimental results, we had to use

their parameter $k$ as a fudge factor, as opposed to its theoretical purpose. From the derivation of Bird's model, $k=1/c$, where $c$ is the scaling factor from **Equation 5**. Previous reports have shown that the value of $c$ is consistent among a variety of different drop impact experiments, and usually remains near $c$=0.7 [7]. Our own results confirm this, since we found that $c$ ranged only from 0.72 to 0.87 for our six different surfaces (full details provided in Supporting Note 2). Bird (2009) found that $k$=2.5 on a smooth glass surface, and asserted that for other experiments, $k$ would remain of order 1 based on its inverse relationship with $c$ [17]. However, as per **Table 2**, our results strongly contradict this statement, since we observed values of $k$ ranging from 4.2 to 94.9 on our t-PTFE and s-Al surfaces, respectively. Therefore, it should be noted that although Bird's model can provide a good fit for the oblique splashing threshold, the value of $k$=2.5 that Bird et al. (2009) reported is applicable only to their own experiment and should not be used for different experimental settings, as has been done unsuccessfully by other researchers [11].

Comparing, Bird's model defines a splashing threshold very similar to our model. As was the case for our model, the only major deviations occur on the smooth surfaces. Specifically, all of the non-splashing aerodynamic breakup points are found above the dashed line for Bird's model, in the splashing region. Thus, comparing our model with Bird's, we note that the two models performed equally well in defining the oblique splashing threshold in the experimental range tested. However, the two models begin to diverge at large values of $v_t$, as the slope of Bird's model decreases, while the slope of our model remains constant. Therefore, a follow-up study at higher maximum sample speeds would cause the models to differ more significantly in their threshold prediction, and would clarify which model is actually more effective.

### 3.3. THE IMPALEMENT TRANSITION ON SUPERHYDROPHOBIC SURFACES

Having modelled the oblique splashing threshold of our surfaces, we now consider the transition from rebounding to partial rebounding behaviour on our SHP surfaces. From our experiments, we found that the critical velocity for pinning at a normal angle of incidence, ($v_{pin,0}$), for the 0.95 mm diameter droplets on the textured PTFE and aluminum surfaces were $v_{pin,0}$=1.86 [1.73; 1.99] and 1.67 [1.52; 1.82] m/s, respectively (as illustrated by the dotted lines shown in both **Figure 4** and **Figure 8**). This threshold is governed by a localized Cassie-to-Wenzel wetting transition at the impact center, and can be predicted by considering the pressure balance between the anti-wetting Laplace pressure ($P_L$) and the impalement pressure of the impacting drop ($P_{imp}$). The raster-scanning method used to synthesize the SHP surfaces tested in this report gave them a crest-and-trough microstructure (see **Figure 2**), with successive crests being spaced 10.53 μm apart, so that $R_L$=5.27 μm for the liquid interface during the impalement process. From **Equation 1** and the advancing contact angles of 157° measured for both textured surfaces, we estimate the Laplace pressures as 25 kPa. Using **Equation 2** and equating $P_{imp}$=$P_L$, we find that the theoretical critical velocity for the impalement transition is $v_{pin,0}$=1.77 m/s for both textured surfaces. This value is exceptionally close to the observed values of $v_{pin,0}$ on our textured surfaces, differing by only about 5% in each case. We suggest that $v_{pin,0}$ was lower on the t-Al surface than on the t-PTFE surface due to the greater inherent adhesion between water and aluminum as compared to PTFE. The difference in adhesion can be quantified by the greater contact angle hysteresis (CAH) of $CAH$=54° measured on our smooth aluminum surface, as compared to $CAH$=27° for smooth PTFE [37].

Although a number of simpler models than Maitra's model (**Equation 2**) have been proposed in order to predict the pinning threshold based on balancing $P_L$ with either the dynamic or water hammer pressure, these models do not include the effect of the droplet diameter [15, 38, 39]. From our own experiments, we observed that water droplets of larger diameter are significantly more

prone to pinning than smaller droplets, which is demonstrated in supporting **Figure S4,** in which one large droplet exhibits partial rebounding behaviour, while two smaller droplets concurrently exhibit complete rebounding. Therefore, seeing that Maitra's model includes the effect of the droplet diameter, and that its prediction is in good agreement with the pinning threshold observed in our experiments, we believe that it is the most appropriate choice of model to describe our results.

The above discussion considers impacts at a normal angle of incidence, however, we found that the critical normal impalement velocity for oblique impacts, $v_{pin}$, is a weak function of the tangential velocity of the impact. As can be seen from the slight slope of the associated line in **Figure 8(e-f)**, $v_{pin}$ increases slightly at higher $v_t$, and can be approximated by the following linear relation:

$$v_{pin} = v_{pin,0} + \omega|v_t|, \tag{9}$$

in which $\omega$ is a fitting factor. Note that since the impalement transition occurs at the impact center as opposed to at the spreading lamella, there is no need to consider positive and negative values of $v_t$ as was done for the splashing threshold, and $v_t$ can simply be taken as its absolute value. For the t-PTFE and t-Al surfaces, we found that $\omega$=0.06 [0.01; 0.11] and $\omega$=0.07 [0.04; 0.10], respectively. Since $v_{pin}$ varies only as a weak function of $v_t$, the impalement transition is governed primarily by $v_n$. This observation is useful industrially, since in application, SHP surfaces are employed in order to reflect droplets from a surface, so impalement is undesired. Our results show that, by angling the SHP surface with respect to the droplet's trajectory, the normal component of the velocity can be reduced to below the impalement threshold, resulting in rebounding behaviour for droplets travelling faster than $v_{pin}$. This phenomenon led to the possibility of stretched rebounding, where the normal velocity of the impact was low enough to prevent impalement and allow rebounding,

while the tangential motion stretched the droplet lengthwise prior to its detachment from the surface.

## 4. CONCLUSIONS

We performed high-speed, oblique drop impacts on six different surfaces: two substrate materials of different inherent surface wettability (PTFE and aluminum), each prepared with three different surface finishes (smooth, rough, and textured). We found that the splashing threshold of oblique drop impacts can be accurately described by considering the normal and tangential components of the impact velocity, and by applying a linear model. Our choice of surfaces has allowed us to make several novel comparisons, including the effects of surface roughness (smooth versus rough), the inherent surface chemistry (PTFE versus aluminum), and the wetting state (Wenzel versus Cassie) on the oblique splashing threshold.

By comparing the normal splashing threshold on the aluminum and PTFE surfaces, we discovered that the inherent surface chemistry of the surface plays an integral role, such that for surfaces of equal roughness, more hydrophobic surfaces encourage splashing. This is a significant finding since, in the past, reports that compared the splashing threshold on different surfaces have only considered the effect of the roughness.

For oblique impacts, we found that the asymmetry of the impact behaviour could be quantified by considering the tangential component of the impact velocity. The tangential velocity played the most prominent role in affecting the impact behaviour on smoother, more hydrophilic surfaces, resulting in one-sided splashing occurring under a wide range of impact conditions. In contrast, we found that on our rough, and especially on our textured (SHP) surfaces, the tangential velocity held much less influence, and the behaviour was governed primarily by the normal impact velocity, resulting in more symmetrical splashing behaviour. We attribute this difference to the low liquid-

solid surface fraction encountered by the spreading lamella on the rough and SHP surfaces, which reduces the drag between the surface and the spreading lamella of the impacting droplet.

By analyzing the critical velocity for pinning on SHP surfaces at different impact angles, we found that the transition is governed primarily by the normal velocity, with only a weak dependence on the tangential velocity, such that the critical normal velocity for pinning ($v_{pin}$) increases slightly in highly oblique impacts. As a result, we observed a new behaviour in highly oblique impacts on SHP surfaces, which we call the stretched rebound. In this case, the droplet is stretched laterally into an elongated pancake shape by the tangential motion of the surface, and rebounds while still out-stretched. Because this behaviour did not involve a recession phase, the contact time with the surface was significantly reduced compared to classic rebounding behaviour. This finding is important for industrial purposes because superhydrophobic surfaces are a promising candidate as anti-icing surfaces, and a reduced contact time is favourable to prevent ice accretion [10].

There are several aspects of our findings in this report that merit follow-up experiments in order to better define the observed trends. Experiments at higher velocity would determine whether our model or the model proposed by Bird et al. (2009) is more effective in predicting the splashing threshold of oblique drop impacts. In addition, drop impact experiments must be performed on surfaces composed of a wider variety of materials, as well as with more defined geometries, in order to better understand how the advancing contact angle and the solid surface fraction affect the oblique splashing threshold. Finally, where we observed a linear relationship between $v_{pin}$ and the tangential impact velocity, curve fitting was performed using relatively few data points, and the defined confidence intervals for the fitting factor ($\omega$) are nearly as large as $\omega$ itself for both surfaces

tested. This indicates that, although $v_{pin}$ certainly depends on the tangential velocity, a more rigorous exploration is required in order to clarify the exact nature of their relationship.

ASSOCIATED CONTENT

Figures: high-speed images of single droplet generated by DOD (Figure S1), simultaneous impact of one large and two small droplets on the t-PTFE surface (Figure S4)

Notes: explanation of the splashing threshold model transformation into Figure 4 (Supporting Note 1), spreading dynamics on different surfaces (Supporting Note 2)

Videos: The original videos of the behaviours shown in Figures 5 and 6

This material is available free of charge via the Internet at http://pubs.acs.org.

AUTHOR INFORMATION

**Corresponding Author**

Anne-Marie Kietzig, McGill University, Department of Chemical Engineering 3610 University Street, Montreal, Quebec, H3A 0C5, Canada, email: anne.kietzig@mcgill.ca.

**Author Contributions**

Damon Aboud designed and performed the experiments, and wrote the manuscript. Prof. Anne-Marie Kietzig guided the project and edited the manuscript. All authors have given approval to the final version of the manuscript.

**Funding Sources**

This work was supported by the Natural Sciences and Engineering Research Council (NSERC) of Canada, and also by the Fonds de recherche du Québec - Nature et technologies (FRQNT).

ACKNOWLEDGMENT

We would like to acknowledge FRQNT and NSERC for their support, as well as the entire Surface Engineering Group of McGill University, including Dr. J. Lehr and F. Liang for their guidance in femtosecond lasing. Also, we thank Prof. Andrew Higgins for his help in realizing the double diaphragm ballistics technique, as well as Dr. Felipe Aristizabal for his help with the logistic regression.

REFERENCES

1. Xu, L., W.W. Zhang, and S.R. Nagel, *Drop splashing on a dry smooth surface.* Phys. Rev. Lett., **2005**. 94(18): p. 184505.
2. Rioboo, R., C. Tropea, and M. Marengo, *Outcomes from a drop impact on solid surfaces.* Atomization Sprays, **2001**. 11(2): p. 155-165.
3. Liu, Y., L. Moevius, X. Xu, T. Qian, J.M. Yeomans, and Z. Wang, *Pancake bouncing on superhydrophobic surfaces.* Nat. Phys., **2014**.
4. Maitra, T., M.K. Tiwari, C. Antonini, P. Schoch, S. Jung, P. Eberle, and D. Poulikakos, *On the nanoengineering of superhydrophobic and impalement resistant surface textures below the freezing temperature.* Nano Lett., **2013**. 14(1): p. 172-182.
5. Stow, C. and M. Hadfield, *An experimental investigation of fluid flow resulting from the impact of a water drop with an unyielding dry surface.* Proc. R. Soc. London, Ser. A, **1981**. 373(1755): p. 419-441.
6. Range, K. and F. Feuillebois, *Influence of surface roughness on liquid drop impact.* J. Colloid Interface Sci., **1998**. 203(1): p. 16-30.
7. Mongruel, A., V. Daru, F. Feuillebois, and S. Tabakova, *Early post-impact time dynamics of viscous drops onto a solid dry surface.* Phys. Fluids, **2009**. 21(3): p. 032101.
8. Kim, H., U. Park, C. Lee, H. Kim, M.H. Kim, and J. Kim, *Drop splashing on a rough surface: How surface morphology affects splashing threshold.* Appl. Phys. Lett., **2014**. 104(16): p. 161608.
9. Peng, C., S. Xing, Z. Yuan, J. Xiao, C. Wang, and J. Zeng, *Preparation and anti-icing of superhydrophobic PVDF coating on a wind turbine blade.* Appl. Surf. Sci., **2012**. 259: p. 764-768.
10. Lv, J., Y. Song, L. Jiang, and J. Wang, *Bio-Inspired Strategies for Anti-Icing.* ACS nano, **2014**.
11. Li, H. *Drop Impact on Dry Surfaces With Phase Change*. Ph.D. Thesis, Technische Universität Darmstadt, **2013**.
12. Li, X.-M., D. Reinhoudt, and M. Crego-Calama, *What do we need for a superhydrophobic surface? A review on the recent progress in the preparation of superhydrophobic surfaces.* Chem. Soc. Rev., **2007**. 36(8): p. 1350-1368.
13. Yeong, Y.H., J. Burton, E. Loth, and I.S. Bayer, *Drop Impact and Rebound Dynamics on an Inclined Superhydrophobic Surface.* Langmuir, **2014**. 30(40): p. 12027-12038.

14. Ramachandran, R., K. Sobolev, and M. Nosonovsky, *Dynamics of Droplet Impact on Hydrophobic/Icephobic Concrete With Potential for Superhydrophobicity.* Langmuir, **2015**.
15. Kwon, H.-M., A.T. Paxson, K.K. Varanasi, and N.A. Patankar, *Rapid deceleration-driven wetting transition during pendant drop deposition on superhydrophobic surfaces.* Phys. Rev. Lett., **2011**. 106(3): p. 036102.
16. Mundo, C., M. Sommerfeld, and C. Tropea, *Droplet-wall collisions: experimental studies of the deformation and breakup process.* Int. J. Multiphase Flow, **1995**. 21(2): p. 151-173.
17. Bird, J.C., S.S. Tsai, and H.A. Stone, *Inclined to splash: triggering and inhibiting a splash with tangential velocity.* New J. Phys., **2009**. 11(6): p. 063017.
18. Liu, J., H. Vu, S.S. Yoon, R.A. Jepsen, and G. Aguilar, *Splashing phenomena during liquid droplet impact.* Atomization Sprays, **2010**. 20(4).
19. Šikalo, Š., C. Tropea, and E. Ganić, *Impact of droplets onto inclined surfaces.* J. Colloid Interface Sci., **2005**. 286(2): p. 661-669.
20. Chen, R. and H. Wang, *Effects of tangential speed on low-normal-speed liquid drop impact on a non-wettable solid surface.* Exp. Fluids, **2005**. 39(4): p. 754-760.
21. Ghai, I., J. Wentz, R.E. DeVor, S.G. Kapoor, and J. Samuel, *Droplet behavior on a rotating surface for atomization-based cutting fluid application in micromachining.* J. Eng. Ind., **2010**. 132(1): p. 011017.
22. Fathi, S., P. Dickens, and F. Fouchal, *Regimes of droplet train impact on a moving surface in an additive manufacturing process.* J. Mater. Process. Technol., **2010**. 210(3): p. 550-559.
23. Zen, T.-S., F.-C. Chou, and J.-L. Ma, *Ethanol drop impact on an inclined moving surface.* Int. Commun. Heat Mass Transfer, **2010**. 37(8): p. 1025-1030.
24. Povarov, O., O. Nazarov, L. Ignat'evskaya, and A. Nikol'Skii, *Interaction of drops with boundary layer on rotating surface.* J. Eng. Phys. Thermophys., **1976**. 31(6): p. 1453-1456.
25. Liang, F., J. Lehr, L. Danielczak, R. Leask, and A.-M. Kietzig, *Robust non-wetting PTFE surfaces by femtosecond laser machining.* Int. J. Mol. Sci., **2014**. 15(8): p. 13681-13696.
26. Cheng, S. and S. Chandra, *A pneumatic droplet-on-demand generator.* Exp. Fluids, **2003**. 34(6): p. 755-762.
27. Yarin, A., *Drop impact dynamics: splashing, spreading, receding, bouncing….* Annu. Rev. Fluid Mech., **2006**. 38: p. 159-192.
28. Richard, D., C. Clanet, and D. Quéré, *Contact time of a bouncing drop.* Nature, **2002**. 417(6891): p. 811.
29. Bird, J.C., R. Dhiman, H.-M. Kwon, and K.K. Varanasi, *Reducing the contact time of a bouncing drop.* Nature, **2013**. 503(7476): p. 385-388.
30. Biance, A.-L., F. Chevy, C. Clanet, G. Lagubeau, and D. Quéré, *On the elasticity of an inertial liquid shock.* J. Fluid Mech., **2006**. 554: p. 47-66.
31. Cossali, G., A. Coghe, and M. Marengo, *The impact of a single drop on a wetted solid surface.* Exp. Fluids, **1997**. 22(6): p. 463-472.
32. Rein, M. and J.-P. Delplanque, *The role of air entrainment on the outcome of drop impact on a solid surface.* Acta mechanica, **2008**. 201(1-4): p. 105-118.
33. Lee, S.Y. and S.U. Ryu, *Recent progress of spray-wall interaction research.* Journal of mechanical science and technology, **2006**. 20(8): p. 1101-1117.
34. Cassie, A. and S. Baxter, *Wettability of porous surfaces.* Trans. Faraday Soc., **1944**. 40(0): p. 546-551.

35. Müller, M. and C. Oehr, *Comments on "an essay on contact angle measurements" by Strobel and Lyons.* Plasma Processes and Polymers, **2011**. 8(1): p. 19-24.
36. Ou, J., B. Perot, and J.P. Rothstein, *Laminar drag reduction in microchannels using ultrahydrophobic surfaces.* Phys. Fluids, **2004**. 16(12): p. 4635-4643.
37. Xiu, Y., L. Zhu, D.W. Hess, and C. Wong, *Relationship between work of adhesion and contact angle hysteresis on superhydrophobic surfaces.* The Journal of Physical Chemistry C, **2008**. 112(30): p. 11403-11407.
38. Reyssat, M., A. Pépin, F. Marty, Y. Chen, and D. Quéré, *Bouncing transitions on microtextured materials.* Europhys. Lett., **2006**. 74(2): p. 306.
39. Jung, Y.C. and B. Bhushan, *Dynamic effects induced transition of droplets on biomimetic superhydrophobic surfaces.* Langmuir, **2009**. 25(16): p. 9208-9218.

EXPLANATORY NOTES

* Roughness values are not reported for the textured surfaces since, due to their wiry texture, roughness measurements cannot provide a relevant characterization of their surface.

** See Supporting Note 1 for an explanation of the model's shape.

*** In order to minimize variability in modelling, the impacts plotted in this figure were performed using a consistent diameter of D=0.95 mm. Where splashing rebound was observed at high sample velocity ($v_s$) for D=1.3 mm on the textured surfaces, it was not observed for the 0.95 mm drops due to experimental limitations in $v_s$.

TOC GRAPHIC

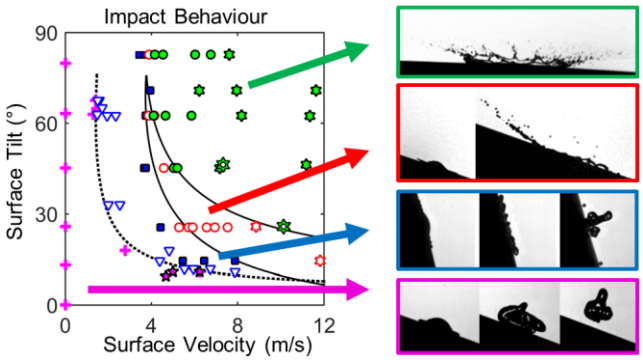


The TOC graphic shows a map of the experimental space, i.e. the speeds and angles tested in oblique water drop impacts on a superhydrophobic sample surface, and the four primary types of behaviours observed: splashing, asymmetrical splashing, breakup, and rebounding. The lines in the plot indicate our models to define the thresholds.